DOI https: //doi. org/10.1007/s11595-020-2268-7

Removal of Chromium (III) from Monoammonium Phosphate Solutions by a Porous Adsorbent of Fluor(calcium silicate) Composites

ZHU Xinhua, JIA Xuhong*

(College of Civil Aviation Safety Engineering, Civil Aviation Flight University of China, Guanghan 618307, China)

Abstract: The products of monoammonium phosphate containing Cr^{3+} resulted in disqualification, and further posed a serious threat to ecological environment and human beings. Herein, the porous adsorbent of fluor(calcium silicate) composites (FCSc) was prepared by hydrothermal method using diatomaceous earth, hydrated lime and additive (NaF) as raw materials, which was characterized and used for the removal of Cr^{3+} from monoammonium phosphate solutions. The effects of different parameters, such as solution pH, initial Cr^{3+} concentration, temperature and contact time on the adsorption of Cr^{3+} onto FCSc were investigated in details. The results indicated that the adsorption process was in agreement with the pseudo-second-order kinetic model and Freundlich isotherm. The spontaneous and endothermic nature of the adsorption process was obtained by analyzing various thermodynamic parameters ($\triangle G^0$, $\triangle H^0$, and $\triangle S^0$). In addition, computational monte carlo simulations between Cr^{3+} ions and FCSc were conducted to elucidate the adsorption mechanism. Such kind of porous adsorbent provided a potential application in the removal of impurities from monoammonium phosphate industry.

Key words: fluor(calcium silicate) composites; monoammonium phosphate solutions; chromium (III); removal; monte carlo simulations

1 Introduction

Monoammonium phosphate is prepared by concentrating monoammonium phosphate solutions which is made from neutralization of wet phosphoric acid and ammonia gas. Monoammonium phosphate was a valuable chemical product has been widely applied in industry and agriculture. However, the heavy metal contaminants including Cr^{3+}, As^{3+}, and Pb^{2+} ions present in phosphate products, resulting in a great threaten to ecological security and human health because of the toxic ions infiltrating into the soil-water environment[1,2]. Although various methods such as solvent extraction, crystallization, ion-exchange, electrodialysis, chemical precipitation, inspissation have been introduced for wet phosphoric acid purification[3-5], there are still some impurities remained in solution. At present, there are many researches on Cr^{3+} removal from aqueous solutions but very limited research works are done from monoammonium phosphate solutions[6,7]. Therefore, the purification of monoammonium phosphate solutions is studied, and the adsorption process is introduced due to its merits of efficiency, economy and simple operation.

Calcium silicate as a frequently-used adsorbent shows an effective adsorbability on adsorbing phosphate from aqueous solutions, in forming apatite[8-11]. Some researchers suggest that adding the additive of fluorine into calcium silicate can improve the stability of apatite, and promote the formation of apatite. Therefore, the adsorbent of fluor(calcium silicate) composites (FCSc) was prepared by hydrothermal method using diatomaceous earth, hydrated lime and additive (NaF) as raw materials. In this work, the intermediate of fluor-hydroxyapatite composites are formed by adsorbing phosphate onto FCSc from monoammonium phosphate solutions, which has shown excellent ions adsorbability and exchangeability[12-15] for most heavy metals in aqueous solutions such as Cd^{2+}, Cr^{3+}, Ni^{2+}, Fe^{3+}, Pb^{2+}, and Zn^{2+}, *etc*[16-19]. The adsorbent FCSc was applied in the removal of Cr^{3+} from monoammonium phosphate solutions and the adsorption parameters such as solution pH, initial Cr^{3+} concentration, temperature

(Received: June 12, 2019; Accepted: Aug. 20, 2019)

ZHU Xinhua (朱新华): Ph D; E-mail: zhuxinhua19@163.com

* Corresponding author: JIA Xuhong (贾旭宏): Assoc. Prof.; Ph D; E-mail: jiaxuhong02@163.com

Funded by the National Natural Science Foundation of China (U1633203), and the Major Project of the Civil Aviation Administration of China (J2020-108)

and contact time were investigated experimentally.

2 Experimental

2.1 Materials

Fluorine-contained silica with the amount of fluoride approximately 10% was obtained from a fluorine plant of Yunnan in China. Hydrated lime (AR grade) was produced by Chengdu Kelong Chemical CO. Ltd., China. Sodium fluoride (GR grade) was produced by Tianjin Guangfu Fine Chemical Research Institute, China. Diatomaceous earth (CP grade) and quartz sand (QS, AR grade) were obtained from Chengdu Jinshan Chemical Co. Ltd., China. Deionized water was produced by Aquapro making water machine (ABZ1-1001-P) in our laboratory.

2.2 Preparation of fluor(calcium silicate) composites

FCSc was prepared as follows: siliceous material (Fluorine-contained silica, diatomaceous earth or quartz sand), calcareous material (Hydrated lime) and additive (NaF) were mixed together with Ca/Si molar ratio of 0.7, and the additive of NaF was calculated based on the amount of fluoride of fluorine-contained silica. The mixture was stirred and treated by wet-milling forming suspension with a water-solid mass ratio of 15, and transferred to a stirred autoclave heated at 160 ℃ for 10 h. Then the FCSc were prepared after filtering, washing by deionized water 3 times and drying at 105 ℃ for 6 h.

2.3 Batch adsorption experiments

Stock solutions of Cr^{3+} (500 mg/L) were prepared by dissolving chromic nitrate nonahydrate in deionized water. simulation solutions was prepared using monoammonium phosphate as raw material with percent content of 8%, and working solutions of Cr^{3+} ranging from 2.5 to 20 mg/L were obtained by diluting the stock solutions with the simulation solutions.

2.4 Desorption experiments

In order to estimate the desorption and resorption performance of Cr^{3+} onto FCSc, the desorption-resorption studies were carried out by adding FCSc (0.3 g) into Cr^{3+} solutions (10 mg/L, 200 mL). The mixture was stirred at 130 r/min, pH of 4.2 and 45℃ for 400 min. And the solid residue was obtained after filtering, which further washed by deionized water 3 times and drying at 105 ℃ for 6 h. After that, the FCSc loaded Cr^{3+} was regenerated by adding separately 50 mL eluents (CH_3COOH, $Ca(NO_3)_2$, EDTA-2Na, and NaOH) into a beaker stirring at 130 r/min at 45 ℃ for 120 min. The percentage desorption (Desorption %) of Cr^{3+} from FCSc was calculated from the following equation:

$$\text{Desorption (\%)} = \frac{\text{Amount of } Cr^{3+} \text{ desorbed to eluents}}{\text{Amount of } Cr^{3+} \text{ adsorbed onto adsorbents}} \times 100\% \quad (1)$$

2.5 Analysis

The morphology and internal structure of adsorbents was examined by a SU3500 scanning electron microscope (Hitachi, Japan). The element composition of adsorbents was analyzed by energy dispersive spectrometer (EDS, Hitachi, Japan). The particle size distribution were determined by laser particle size distribution analyzer (BT-9300S, China). The Brunauer Emmett Teller specific surface area was measured from N_2 adsorption-desorption isotherms using a KUBO-X1000 adsorption analyzer (Builder, China).

The concentration of Cr^{3+} was detected by diphenylcarbohydrazide spectrophotometry method (GB 7466-87) equipped with a ultraviolet spectrophotometer (UV-1100). The linear equation of standard curve (Y=1.6274X+0.0018, R^2=0.9995) was obtained in the experiment, and the adsorption amount of chromium (q_e, mg/g) adsorbed on FCSc and the removal percentage (removal, %) of Cr^{3+} ions from monoammonium phosphate solutions were calculated using the following equations:

$$q_e = \frac{(C_0 - C_e) \times V}{m} \quad (2)$$

$$\text{Removal (\%)} = \frac{C_0 - C_e}{C_0} \times 100\% \quad (3)$$

where, C_e (mg/L) is the equilibrium Cr^{3+} concentration in solution, C_0 (mg/L) is the initial Cr^{3+} concentration in solution, m (g) is the mass of adsorbent and V (L) is the volume of the solution.

3 Results and discussion

3.1 Characterization of fluor(calcium silicate) composites

Siliceous materials had an important effect on the adsorption of Cr^{3+} on FCSc from monoammonium phosphate solutions, and the results are shown in Table 1 and Fig.1. The mean diameter and specific surface area varied with siliceous materials according to Table 1. The adsorbent D with smaller specific surface area exhibited poor adsorbability for Cr^{3+} ions (Fig.1) although it showed a smaller surface mean diameter (*SMD*), the reason was that there were few micro-pores

on the surface and inner of the adsorbent. Adsorbents A, B, and C showed excellent adsorbability for Cr^{3+} ions and the removal rate more than 60%. However, the adsorbent C with the small specific surface area (52.40 m^2/g) exhibited excellent adsorbability for Cr^{3+} ions due to the higher reactivity of fluorine-contained silica than others. Furthermore, the activated carbon and porous carbon were widely used as adsorption materials, which showed good adsorbability for metal ions because of its large specific surface area[20,21]. The specific surface area of adsorbent B was higher than adsorbent A due to blending with activated carbon. However, the adsorption amount of adsorbent B was lower than A, because FCSc adsorbed Cr^{3+} ions via chemisorption but the activated carbon was physisorption.

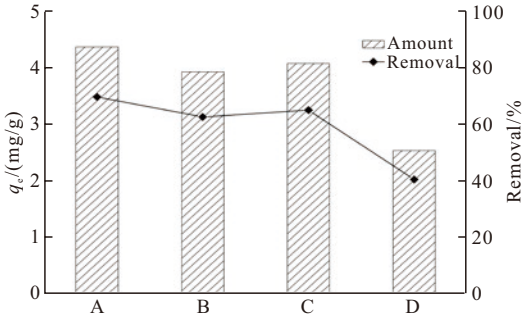

Fig.1 The adsorption effects of Cr^{3+} on different adsorbents. Amount of adsorbents, 0.3 g/L; initial Cr^{3+} concentration, 10 mg/L; agitation speed, 130 r/min; solution pH, 4.2; adsorption time, 400 min; solution temperature, 45℃

The N_2 adsorption-desorption isotherm of the FCSc is presented in Fig.2. The adsorbent showed the type I isotherm as defined by IUPAC classification with the H_3 hysteresis loop, indicated the presence of mesopores[22,23]. The porous morphologies of adsorbent A with different magnifications are shown in Fig.3. It could be found that FCSc exhibited well-developed space connected cellular structure with a higher surface area of 123.62 m^2/g (Table 1), which could provide more adsorption and ion exchange sites[24]. Therefore, the adsorbent A was chosen for adsorption process in this work and used for further adsorption experiments.

3.2 Effect of pH

It was found that the peak of chromium appeared in the EDS spectra from Fig.4 indicating the adsorbent loaded with Cr^{3+} ions after adsorption. According to Table 2, the calcium atomic ratio of adsorbent decreased more than 70% after adsorption due to the ion-exchange mechanism and partially dissolution of adsorbent in weak acidic. As a result, the Cr^{3+} adsorption onto FCSc from monoammonium phosphate solutions was feasible and the solution pH was an important effect for Cr^{3+} adsorption.

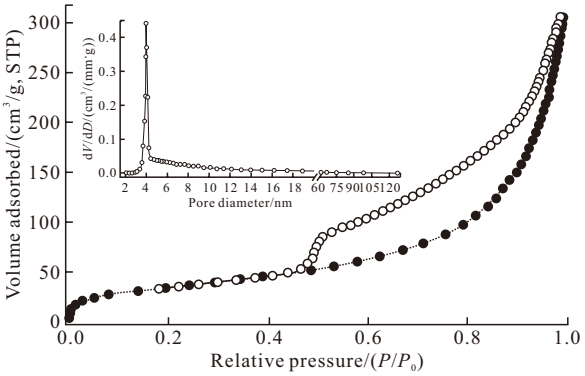

Fig.2 N_2 adsorption-desorption isotherm curves of FCSc

The effect of initial solution pH on the adsorption of Cr^{3+} onto FCSc was carried out. The pH value in the range of 2.7-4.7 was chosen based on the reason that Cr^{3+} started to precipitate when the pH was higher than 4.7 according to solubility of chromic hydroxide[25]. As shown in Fig.5, the adsorption of Cr^{3+} onto FCSc was

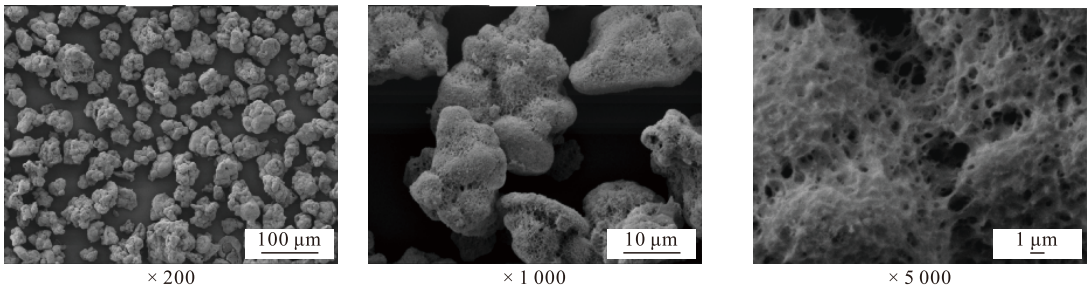

× 200 × 1 000 × 5 000

Fig.3 The porous morphologies of FCSc by scanning electron microscopy

Table 1 Characterization of adsorbents with different siliceous materials

Adsorbents	Siliceous materials	Mean diameter/μm			Surface area/(m^2/g)
		*D*50	*D*90	*SMD*	
A	Diatomaceous earth	33.16	61.24	14.51	123.62
B (Blending with activated carbon)	Diatomaceous earth	26.40	51.05	11.96	155.35
C	Fluorine-contained silica	10.04	23.38	7.772	52.40
D	Quartz sand	12.27	32.64	5.344	20.57

Table 2 EDS analysis: element composition of FCSc adsorbent before and after Cr^{3+} adsorption

Elements	Before adsorption		After adsorption	
	Weight/%	Atomic/%	Weight/%	Atomic/%
Oxygen	48.51	66.33	53.31	68.85
Fluorine	2.64	1.87	1.70	0.62
Silicon	20.66	16.09	29.21	21.49
Calcium	26.95	14.71	8.08	4.17
Aluminum	1.24	1.00	1.88	1.44
Phosphorous	-	-	4.14	2.76
Chromium	-	-	1.68	0.67

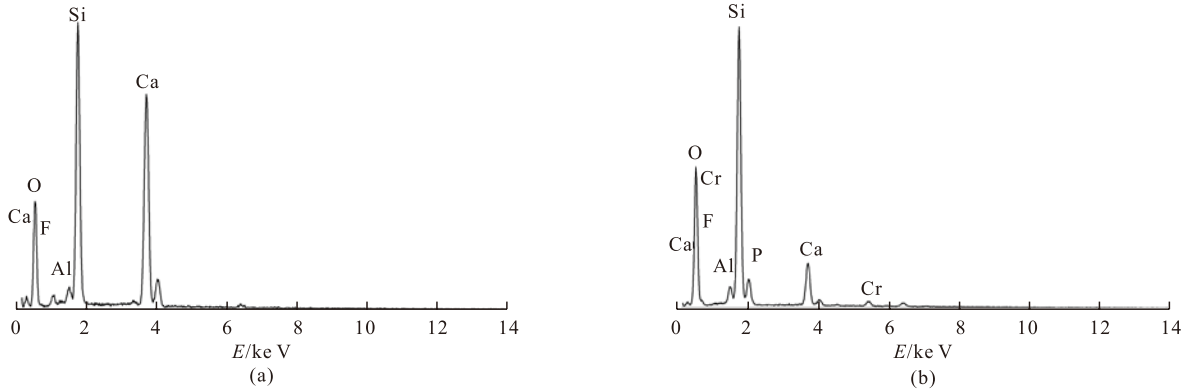

Fig.4 EDS spectra of FCSc adsorbent (a) before and (b) after Cr^{3+} adsorption

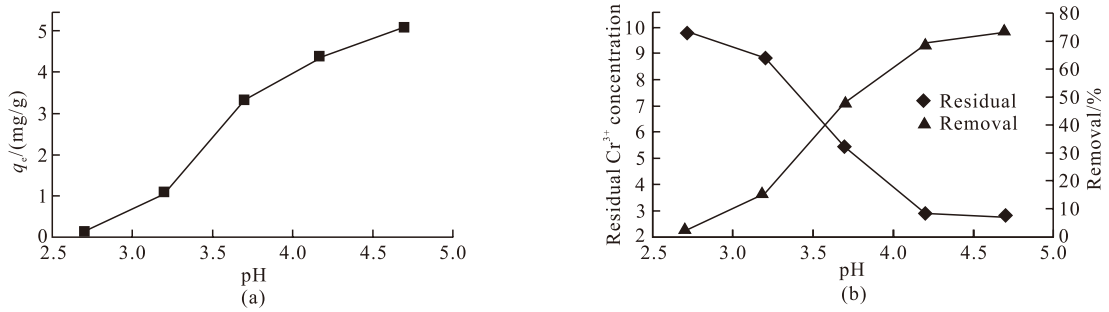

Fig.5 Effects of solution pH on the adsorption of Cr^{3+} onto FCSc. Amount of adsorbent FCSc, 0.3 g/L; initial Cr^{3+} concentration, 10 mg/L; agitation speed, 130 r/min; adsorption time, 400 min; solution temperature, 45℃

highly dependent on solution pH, which was attributed to the fact that solution pH affected the solubility of metal ions and ionization state of the functional groups presented on the adsorbents[26]. The Cr^{3+} adsorption increased from 0.13 to 5.07 mg/g within the range of pH 2.7-4.7. The residual Cr^{3+} concentration was below 2.85 mg/L with the removal rate up to 73.41% when the solution pH was higher than 4.2. Therefore, the solution pH of 4.2 was chosen for further adsorption experiments in this work.

3.3 Effect of initial Cr^{3+} concentration

The effect of initial Cr^{3+} concentration on the adsorption of Cr^{3+} onto FCSc is shown in Fig.6. It was found that the amount of Cr^{3+} ions adsorbed onto FCSc increased with the increase of initial Cr^{3+} concentration. The Cr^{3+} adsorption of 8.73 mg/g was obtained as the initial concentration up to 20 mg/L, and the removal rate of Cr^{3+} was more than 68% with different concentrations. The residual concentration was below 2.0 mg/L and even down to 0.69 mg/L with an initial concentration of Cr^{3+} ions below 7.5 mg/L. The Cr^{3+} ions

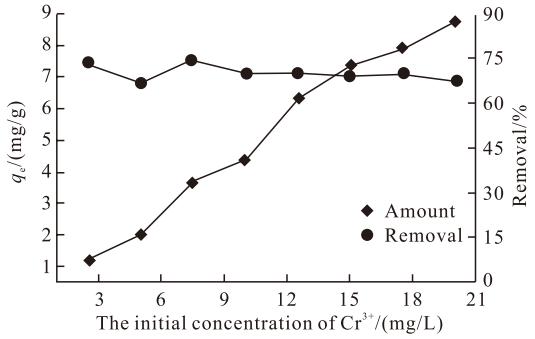

Fig.6 Effect of the initial Cr^{3+} concentration on the adsorption of FCSc for Cr^{3+}. Amount of adsorbent FCSc, 0.3 g/L; agitation speed, 130 r/min; solution pH, 4.2; adsorption time, 400 min; solution temperature, 45℃

started to precipitate with PO_4^{3-} in monoammonium phosphate solutions as the initial concentration of Cr^{3+} was over 20 mg/L. Therefore, FCSc was an excellent adsorbent for the removal of Cr^{3+} concentration below 20 mg/L.

3.4 Adsorption isotherms

The Langmuir and Freundlich isotherms were usually used to describe the equilibrium between metal ions adsorbed onto adsorbents and metal ions in solution. The Langmuir and Freundlich isotherms assume a monolayer adsorption and heterogeneous adsorption process, respectively, and the linear forms of both isotherm equations are given by Eqs. (4) and (5):

$$\frac{C_e}{q_e}=\frac{1}{K_L q_m}+\frac{C_e}{q_m} \tag{4}$$

$$\ln q_e=\ln K_f+\frac{1}{n}\ln C_e \tag{5}$$

where, q_e (mg/g) is the adsorption of Cr^{3+} adsorbed at equilibrium, C_e (mg/L) is the equilibrium concentration of Cr^{3+} in solution, q_m (mg/g) is the maximum adsorption representing monolayer coverage of adsorbent with adsorbate, K_L (L/mg) is the Langmuir coefficient related to surface adsorption energy, K_f (mg/g) is the Freundlich constant related to the adsorption amount and n is the intensity of adsorption. Additionally, a dimensionless constant R_L reflects the essential characteristic of Langmuir model and can be calculated using the Eq. (6):

$$R_L=\frac{1}{1+K_L C_0} \tag{6}$$

where, C_0 (mg/L) is the initial concentrations of Cr^{3+} ions in solution.

The experiment adsorption data were fitted using Langmuir and Freundlich isotherms and the results were presented in Fig.7 and Table 3. Based on Fig.7 and Table 3, the correlation coefficient for Freundlich model was more than 0.98, suggesting that the adsorption of Cr^{3+} onto FCSc was well described by Freundlich isotherm model. The numerical value of n^{-1} smaller than 1.0 demonstrated that the Cr^{3+} adsorption was only slightly decreased at lower equilibrium concentrations, and the isotherm did not predict any saturation of the sorbent by the sorbate[27,28]. The reason was attributed to the heterogeneous nature of active sites on the surface of adsorbent and a multilayer adsorption occurred between adsorbent and Cr^{3+}.

Table 3 Kinetic parameters of Cr^{3+} adsorption onto FCSc

Adsorbent	FCSc
Langmuir isotherm	
q_m/(mg/g)	32.68
K_L/(L/mg)	0.0584
R_L	0.6313
R^2	0.7570
Freundlich isotherm	
K_f/ (mg/g)	1.7873
n^{-1}	0.8876
R^2	0.9886

3.5 Effect of temperature and adsorption thermodynamics

The effect of temperature on the adsorption of Cr^{3+} onto FCSc was studied at 288, 298, 308, and 318 K. The results showed that the Cr^{3+} adsorption increased with increase in temperature, indicating that the adsorption process was endothermic in nature.

Thermodynamic parameters are calculated using the following equations:

$$\ln K_d=\frac{\Delta S^0}{R}-\frac{\Delta H^0}{RT} \tag{7}$$

$$\Delta G^0=-RT\ln K_d \tag{8}$$

The linear fit of thermodynamics for the adsorption process is shown in Fig.8. According to Fig.8, the enthalpy change of $\triangle H^0$ was calculated to be 89.60 kJ/mol, suggesting the endothermic nature of the adsorption process and demonstrating the chemisorption

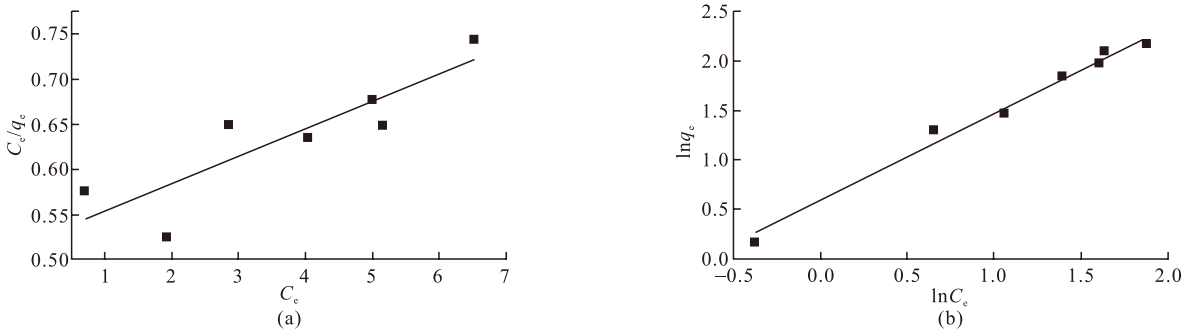

Fig.7 Linear fits of experimental data obtained using Langmuir (a) and Freundlich (b) isotherms for the adsorption of Cr^{3+} onto FCSc

process due to the adsorption heat between 20 and 400 kJ/mol[29]. The Gibbs free energy of $\triangle G^0$ was calculated to be −8.86, −14.10, −16.57, and −19.39 kJ/mol for the adsorption process at 288, 298, 308, and 318 K, respectively. The negative values of $\triangle G^0$ at different temperature indicated the feasibility of the process and spontaneous nature of the adsorption. The $\triangle S^0$ value was found to be 344.18 J/(mol·K) indicating that the degrees of freedom increased at the solid-liquid interface during the adsorption.

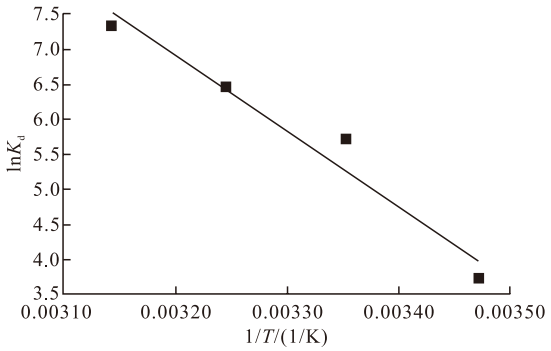

Fig.8 Linear fit of experimental data obtained by plotting of $\ln K_d$ versus $1/T$ for Cr^{3+} adsorption onto FCSc. Amount of adsorbent FCSc, 0.3 g/L; initial Cr^{3+} concentration, 10 mg/L; agitation speed, 130 r/min; solution pH, 4.2; adsorption time, 400 min

3.6 Effect of contact time and adsorption kinetics

Fig.9 shows the effect of contact time on the Cr^{3+} adsorption onto FCSc. It was found that the Cr^{3+} adsorption increased with increase in contact time, and the adsorption equilibrium was achieved in 400-600 min. In addition, the removal rate of Cr^{3+} ions increased with increasing the contact time, and the removal rate was more than 76.17% with the contact time up to 400 min. Therefore, a time of 400 min was chosen for Cr^{3+} adsorption process.

The pseudo-first-order and pseudo-second-order kinetic models are applied in the Cr^{3+} adsorption process, and the equations are given as follows:

$$\ln(q_e - q_t) = \ln q_e - K_1 t \tag{9}$$

$$\frac{t}{q_t} = \frac{1}{K_2 q_e^2} + \frac{t}{q_e} \tag{10}$$

where, q_e (mg/g) is the adsorption of Cr^{3+} ions adsorbed onto adsorbents at equilibrium, q_t (mg/g) is the adsorption of Cr^{3+} ions adsorbed onto adsorbents at time t (min), K_1 (min^{-1}) and K_2 (g/(mg·min)) are the constants of the pseudo-first-order and pseudo-second-order adsorption, respectively.

The intraparticle diffusion equation is used to explore the behavior of intraparticle diffusion of Cr^{3+} ions onto adsorbents, and the equation is given by Eq.(11):

$$q_t = K_p t^{0.5} + C \tag{11}$$

where, K_p (mg/(g·$min^{1/2}$)) is the intraparticle diffusion rate constant.

The experimental data were fitted by the aforementioned kinetic models, and the results are shown in Figs.10, 11 and Table 4. From Fig.10 and Table 4, the obtained R^2 value was higher than 0.99 and the theoretical q_e value was consistent with the experimental value, indicating that the adsorption of Cr^{3+} onto FCSc was well described by the pseudo-second-order kinetic model. These results suggested that the chemisorption was the rate-limiting step in adsorption process. Fig.11 shows the plot of q_t versus $t^{0.5}$ for the adsorption of Cr^{3+} onto FCSc, it was found that the plots were mult-linearity over the whole time range indicating that three steps

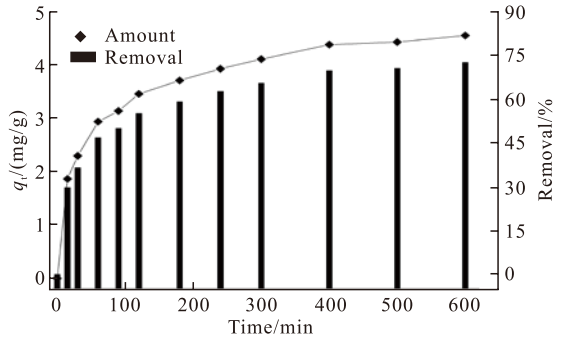

Fig.9 Effect of contact time on the adsorption of Cr^{3+} onto FCSc. Amount of adsorbent FCSc, 0.3 g/L; initial concentration, 10 mg/L; agitation speed, 130 r/min; solution pH, 4.2; solution temperature, 45℃

Table 4 Kinetic parameters of Cr^{3+} adsorption onto FCSc

Adsorbent	FCSc
Pseudo-first order	
q_e/(mg/g)	2.55
K_1/(1/min)	0.0032
R^2	0.9555
Pseudo-second order	
q_e/(mg/g)	4.77
K_2/(g/mg·min)	0.0051
R^2	0.9977
Intraparticle diffusion	
K_{p1}/(mg/(g·$min^{1/2}$))	0.2321
R^2	0.9771
K_{p2}/(mg/(g·$min^{1/2}$))	0.1010
R^2	0.9997
K_{p3}/(mg/(g·$min^{1/2}$))	0.0375
R^2	0.9327

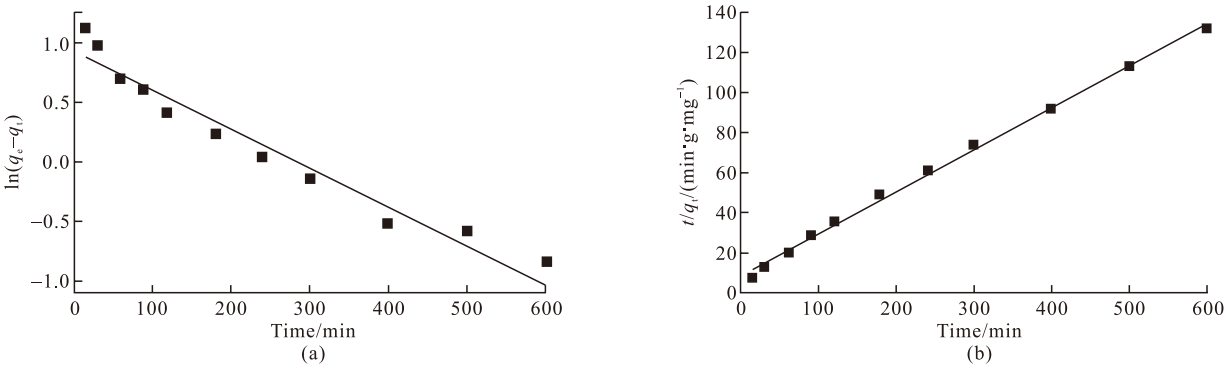

Fig.10 The linearized (a) pseudo-first-order and (b) pseudo-second-order kinetic plots for Cr^{3+} adsorption onto FCSc

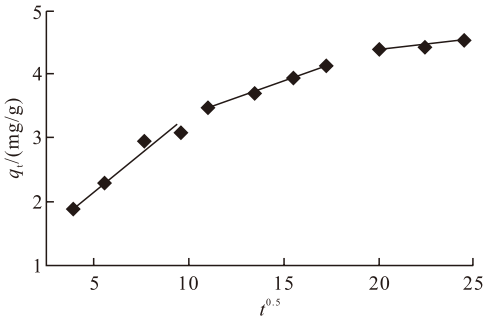

Fig.11 Intraparticle diffusion model for the adsorption of Cr^{3+} onto FCSc

were operational in adsorption. The first linear plot was attributed to rapid external diffusion, the second stage was the rate limiting step, and the third portion was the final equilibrium due to extremely low Cr^{3+} concentration in solution. Based on the results, it was indicated that the adsorption of Cr^{3+} onto FCSc was dominated by chemisorption and intraparticle diffusion.

3.7 Mechanism of Cr^{3+} adsorption

There were two aspects for the adsorption of Cr^{3+} onto FCSc from monoammonium phosphate solutions. On the one hand, the small amount of PO_4^{3-} ionized by $H_2PO_4^-$ combined with Cr^{3+} forming the complex $CrPO_4{\cdot}4H_2O$. And the equations are described as follows:

$$NH_4H_2PO_4 \rightarrow NH_4^+ + H_2PO_4^- \quad (12)$$

$$H_2PO_4^- \leftrightharpoons HPO_4^{2-} + H^+ \quad K_{a2}=6.2\times10^{-8} \quad (13)$$

$$HPO_4^{2-} \leftrightharpoons PO_4^{3-} + H^+ \quad K_{a3}=2.2\times10^{-13} \quad (14)$$

$$PO_4^{3-} + Cr^{3+} \rightarrow CrPO_4{\cdot}4H_2O \text{ (complex)} \quad (15)$$

From equation (14), the concentration of PO_4^{3-} ions was always negligible for high acid concentration. However, the amount of OH^- ions increased with the increasing of solution pH, and the amount of PO_4^{3-} ions increased because of the ionization process favorably shift equilibrium. As the solution pH up to 4.2, the free ions of Cr^{3+} decreased due to the complex $CrPO_4{\cdot}4H_2O$ according to equation (15), which affected the adsorption efficiency of FCSc for Cr^{3+} ions. On the other hand, the adsorbent of FCSc was converted into intermediate fluor-hydroxyapatite (FHA, major component) and adsorbed Cr^{3+} ions simultaneously by ion-exchange. The adsorption process is realized as follows:

$$FCSc+H_2PO_4^-/HPO_4^{2-}/PO_4^{3-} \rightarrow FHA\text{-}Ca^{2+} \quad (16)$$

$$FHA\text{-}Ca^{2+} + Cr^{3+} \rightarrow FHA\text{-}Cr^{3+} + Ca^{2+} \quad (17)$$

In order to validate the formation mechanism of the process, it was investigated that the ideal structure model of Cr^{3+} ions adsorbed on FCSc based on monte carlo simulations.

The hydrated Cr^{3+} ions was one of the most stable complex in aqueous solution, and the octahedral structure of $[Cr(H_2O)_6]^{3+}$ acted as the dominant species of Cr^{3+} ions in aqueous system[30]. The adsorbent FCSc adsorbed phosphate forming fluor-hydroxyapatite, and then adsorbed $[Cr(H_2O)_6]^{3+}$ from monoammonium phosphate solutions. It was found that the structure of fluor-hydroxyapatite was similar to hydroxyapatite in our previous study. Therefore, to model the surface of fluor-hydroxyapatite, a slab of finite thickness was created by cleaving the hydroxyapatite crystal. The hydroxyapatite (100) surface was a valuable cleavage surface, and the morphology and reactivity of the surface were investigated in this work. The computational monte carlo simulations between Cr^{3+} ions and hydroxyapatite were implemented using Materials Studio. The slab was separated from the image in the neighboring cells by a certain vacuum width of 20 Å, and a (2×2×1) supercell of 176 atoms to mimic the hydroxyapatite surface. The production steps was 10^7, temperature was set to 298 K, and the Universal force field was employed to describe the Cr^{3+} adsorption process. The density distribution of $[Cr(H_2O)_6]^{3+}$ on hydroxyapatite (100) surface is shown in Fig.12, it was found that the

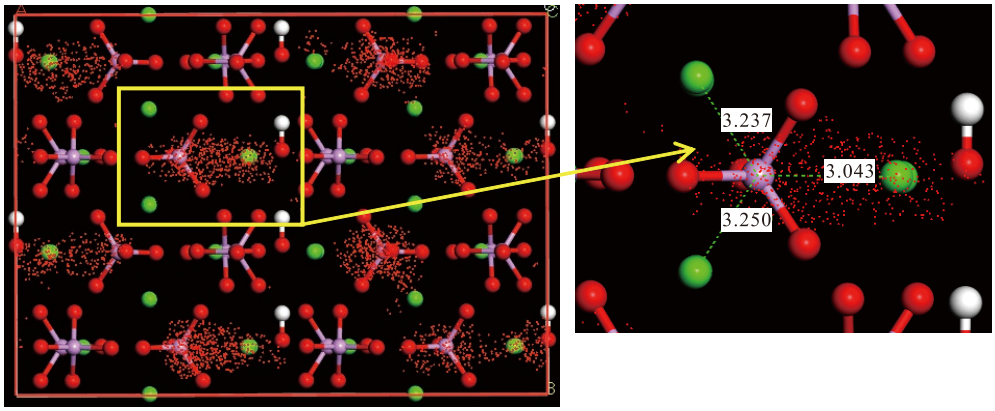

Fig.12 Density distribution of $[Cr(H_2O)_6]^{3+}$ on hydroxyapatite (100) surface at 100 kPa and 298 K. The dots represent $[Cr(H_2O)_6]^{3+}$, the balls represent hydroxyapatite (100) surface (unconnected balls represent Ca^{2+})

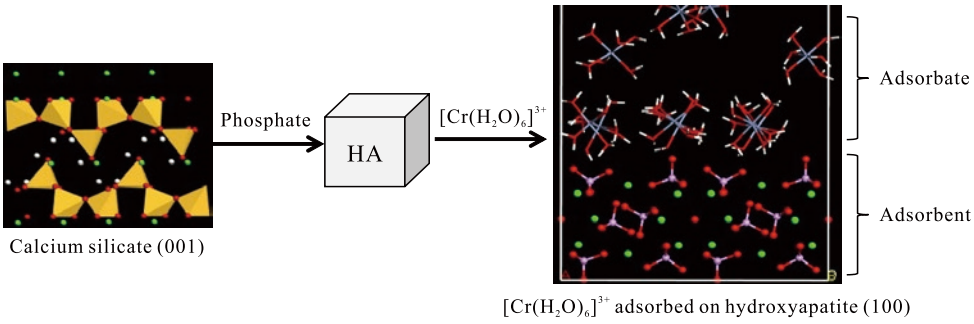

Fig.13 The ideal structure model of $[Cr(H_2O)_6]^{3+}$ on hydroxyapatite (100) surface: the sticks represent $[Cr(H_2O)_6]^{3+}$

adsorption sites of $[Cr(H_2O)_6]^{3+}$ located in the region of P-Ca bond length below 3.043 Å, which indicated the possibility of old P-Ca bond breaking and new P-Cr bond forming. The ideal structure model of $[Cr(H_2O)_6]^{3+}$ on hydroxyapatite (100) surface is presented in Fig.13, which exhibited that the adsorption process of Cr^{3+} onto FCSc involved two steps. FCSc adsorbed phosphate forming hydroxyapatite, and then $[Cr(H_2O)_6]^{3+}$ adsorbed on hydroxyapatite surface by ion-exchange.

3.8 Desorption-resorption experiments

In order to investigate the potential of FCSc for industrial application, desorption-resorption experiments were studied by the batch method using different eluents including CH_3COOH, $Ca(NO_3)_2$, EDTA-2Na, and NaOH. The desorption-resorption results of different eluents for FCSc are shown in Fig.14. From Fig.14, the highest desorption value closed to 100% for Cr^{3+} using EDTA-2Na (0.05 M) as eluent, but the highest resorption value for Cr^{3+} (76.8%) was obtained using EDTA-2Na (0.0025 M) solution. This phenomenon could be explained that the desorption and resorption of Cr^{3+} onto FCSc would be affected by EDTA-2Na concentration. The resorption value was below 29% with high concentration EDTA-2Na (0.05 M) because that Cr^{3+} and Ca^{2+} ions in adsorbent skeleton released simultaneously resulting in adsorbent skeleton breakdown, and the active adsorption sites occupied by excess EDTA-2Na reducing adsorbability due to the strong chelation between EDTA-2Na with cations on FCSc. Moreover, the resorption value was increased with the decrease of EDTA-2Na concentration. The resorption value reached the maximum of 76.8% with EDTA-2Na concentration decreased to 0.0025 M, while the value began to fall with EDTA-2Na concentration reducing to 0.001 M because the fewer EDTA-2Na ions were not be enough to desorb all Cr^{3+} on FCSc reducing resorption performance.

Form Fig.14, it was found that NaOH solution showed a poor performance for Cr^{3+} desorption and resorption. Furthermore, the desorption value of CH_3COOH and $Ca(NO_3)_2$ solutions was below 16%, while

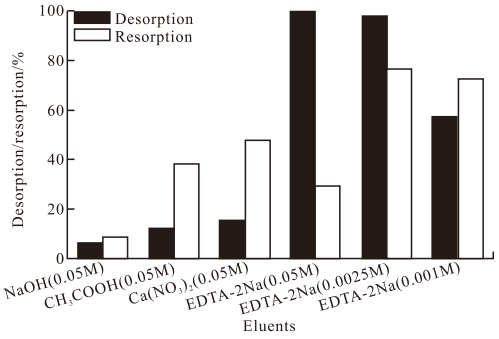

Fig.14 Desorption-resorption efficiencies of Cr^{3+} onto FCSc from monoammonium phosphate solutions

the resorption value was more than 38%, this phenomenon could be explained that the surface ions on FCSc were desorbed only. However, enough active sites exposed after desorption due to high specific surface area of FCSc (Table 1 and Fig.2) increasing the resorption value, which was similar to the desorption and resorption process of low EDTA-2Na concentration (0.001 M). From the above, EDTA-2Na (0.0025 M) was the best eluent for Cr^{3+} desorption-resorption process.

4 Conclusions

The porous adsorbent of FCSc was prepared, characterized and used for the removal of Cr^{3+} ions from monoammonium phosphate solutions. The factors affecting the adsorption process were investigated, and the results showed that FCSc adsorbed Cr^{3+} ions was best fitted the Freundlich isotherm model. The adsorption kinetics were found to follow the pseudo-second-order kinetic model and the plots of intraparticle diffusion were mult-linearity over the whole time range, suggesting that the adsorption of Cr^{3+} onto FCSc was dominated by chemisorption and intraparticle diffusion. The thermodynamic parameters showed that the Cr^{3+} adsorption was spontaneous and endothermic in nature. Based on the results of monte carlo simulations, the adsorption process of Cr^{3+} onto FCSc involved two steps. FCSc adsorbed phosphate forming hydroxyapatite, and then $[Cr(H_2O)_6]^{3+}$ ions adsorbed on hydroxyapatite surface by ion-exchange. Furthermore, the residual Cr^{3+} concentration was below 2.0 mg/L and even down to 0.69 mg/L with an initial Cr^{3+} concentration below 7.5 mg/L. The maximum adsorption of FCSc for Cr^{3+} ions was 8.73 mg/g with an initial Cr^{3+} concentration up to 20 mg/L. Therefore, FCSc was an excellent adsorbent for the removal of Cr^{3+} concentration below 20 mg/L.

References

[1] Lin S, Lian C, Xu M, *et al*. Study on Competitive Adsorption Mechanism among Oxyacid-type Heavy Metals in Co-existing System: Removal of Aqueous As(V), Cr(III) and As(III) Using Magnetic Iron Oxide Nanoparticles (MIONPs) as Adsorbents[J]. *Appl. Surf. Sci.*, 2017, 422: 75-681

[2] Duruibe JO, Ogwuegbu MOC, Egwurugwu JN. Heavy Metal Pollution and Human Biotoxic Effects[J]. *Int. J. Phys. Sci.*, 2007, 2: 112-118

[3] El-Bayaa AA, Badawy NA, Gamal AM, *et al*. Purification of Wet Process Phosphoric Acid by Decreasing Iron and Uranium Using White Silica Sand[J]. *J. Hazard. Mater.*, 2011, 190: 324-329

[4] Hannachi A, Habaili D, Chtara C, *et al.* Purification of Wet Process Phosphoric Acid by Solvent Extraction with TBP and MIBK Mixtures[J]. *Sep. Purif. Technol.*, 2007, 55: 212-216

[5] Awwad NS, El-Nadi YA, Hamed MM. Successive Processes for Purification and Extraction of Phosphoric Acid Produced by Wet Process[J]. *Chem. Eng. Process.*, 2013, 74: 69-74

[6] Ciopec M, Davidescu CM, Negrea A, *et al*. Adsorption Studies of Cr(III) Ions from Aqueous Solutions by DEHPA Impregnated onto Amberlite XAD7-factorial Design Analysis[J]. *Chem. Eng. Res. Des.*, 2012, 90: 1 660-1 670

[7] Kocaba S, Akcin G. Removal of Chromium(III) and Cadmium(II) from Aqueous Solutions[J]. *Desalination*, 2005, 180: 151-156

[8] Renman A, Renman G. Long-term Phosphate Removal by the Calcium-silicate Material Polonite in Wastewater Filtration Systems[J]. *Chemosphere*, 2010, 79: 659-664

[9] Okano K, Uemoto M, Kagami J, *et al*. Novel Technique for Phosphorus Recovery from Aqueous Solutions Using Amorphous Calcium Silicate Hydrates (A-CSHs)[J]. *Water Res.*, 2013, 47: 2 251-2 259

[10] Liu Y, Sheng X, Dong YH, *et al*. Removal of High-concentration Phosphate by Calcite: Effect of Sulfate and pH[J]. *Desalination*, 2012, 289: 66-71

[11] Zhu XH, Zhang Z, Shen J. Kinetics and Mechanism of Adsorption of Phosphate on Fluorine-containing Calcium Silicate[J]. *J. Wuhan Univ. Technol.*, 2016, 31: 321-327

[12] Simon FG, Biermann V, Peplinski B. Uranium Removal from Groundwater Using Hydroxyapatite[J]. *Appl. Geochem.*, 2008, 23: 2 137-2 145

[13] Sundaram CS, Viswanathan N, Meenakshi S. Defluoridation Chemistry of Synthetic Hydroxyapatite at Nano Scale: Equilibrium and Kinetic Studies[J]. *J. Hazard. Mater.*, 2008, 155: 206-215

[14] Krestou A, Xenidis A, Panias D. Mechanism of Aqueous Uranium(VI) Uptake by Hydroxyapatite[J]. *Miner. Eng.*, 2004, 17: 373-381

[15] Feng Y, Gong JL, Zeng GM, *et al*. Adsorption of Cd(II) and Zn(II) from Aqueous Solutions Using Magnetic Hydroxyapatite Nanoparticles as Adsorbents[J]. *Chem. Eng. J.*, 2010, 162: 487-494

[16] Gómez del Río J, Sanchez P, Morando PJ, *et al*. Retention of Cd, Zn and Co on Hydroxyapatite Filters[J]. *Chemosphere*, 2006, 64: 1 015-1 020

[17] Wakamura M, Kandori K, Ishikawa T. Surface Composition of Calcium Hydroxyapatite Modified with Metal Ions[J]. *Colloid. Surface. A*, 1998, 142: 107-116

[18] Kousalya GN, Gandhi MR, Sundaram CS, *et al*. Synthesis of Nano-hydroxyapatite Chitin/Chitosan Hybrid Biocomposites for the Removal of Fe(III)[J]. *Carbohyd. Polym.*, 2010, 82: 594-599

[19] Aliabadi M, Irani M, Ismaeili J, *et al*. Design and Evaluation of Chitosan/Hydroxyapatite Composite Nanofiber Membrane for the Removal of Heavy Metal Ions from Aqueous Solution[J]. *J. Taiwan. Inst. Chem. E.*, 2014, 45: 518-526

[20] Maneechakr P, Karnjanakom S. Adsorption Behaviour of Fe(II) and Cr(VI) on Activated Carbon: Surface Chemistry, Isotherm, Kinetic and Thermodynamic Studies[J]. *J. Chem. Thermodyn.*, 2017, 106: 104-112

[21] Yu F, Wang MJ, Huang BC, *et al*. Acid-treatment Effect on the N-doped Porous Carbon Obtained from Fish Scales for Cr(VI) Removal[J]. *Chem. Pap.*, 2017, 71: 2 261-2 269

[22] Kruk M, Jaroniec M. Gas Adsorption Characterization of Ordered Organic-inorganic Nanocomposite Materials[J]. *Chem. Mater.*, 2001, 13: 3 169-3 183

[23] Singh J, Bhunia H, Basu S. CO_2 Adsorption on Oxygen Enriched Porous Carbon Monoliths: Kinetics, Isotherm and Thermodynamic Studies[J]. *J. Ind. Eng. Chem.*, 2018, 60: 321-332

[24] Zhu XH, Zhang Z, Shen J. Preparation of Calcium Silicate Using Hazardous Solid Wastes and Its Application in Treatment of Phosphate-containing Wastewater[C]. In: *2014 International Conference on Material Science and Environmental Engineering*. Switzerland: Trans Tech Publications, 2014: 652-658

[25] Dean JA. *LANGE'S Handbook of Chemistry*[M]. 15th Edition. New York: McGraw-Hill Compamies, Inc., 1998

[26] Li XL, Li YF, Zhang SD, *et al*. Preparation and Characterization of New Foam Adsorbents of Poly(vinyl alcohol)/Chitosan Composites and Their Removal for Dye and Heavy Metal from Aqueous Solution[J]. *Chem. Eng. J.*, 2012, 183: 88-97

[27] Memon SQ, Bhanger MI, Hasany SM, *et al*. Sorption Behavior of Impregnated Styrofoam for the Removal of Cd(II) Ions[J]. *Colloid. Surface. A*, 2006, 279: 142-148

[28] Zhu XH, Li J, Luo JH, *et al*. Removal of Cadmium (II) from Aqueous Solution by a New Adsorbent of Fluor-hydroxyapatite Composites[J]. *J. Taiwan Inst. Chem. E.*, 2017, 70: 200-208

[29] Ünlü N, Mustafa E. Removal of Heavy Metal Ions by Using Dithiocarbamated- sporopollenin[J]. *Sep. Purif. Technol.*, 2007, 52: 461-469

[30] Chinapong K, Kristof P, Bernd MR. Structure and Dynamics of the Cr(III) Ion in Aqueous Solution: Ab Initio QM/MM Molecular Dynamics Simulation[J]. *J. Comput. Chem.*, 2004, 25: 1 576-1 583